

# EXPERIMENTAL STUDY OF POLYMER ELECTROLYTE MEMBRANE FUEL CELLS USING A GRAPHITE COMPOSITE BIPOLAR PLATE FABRICATED BY SELECTIVE LASER SINTERING

Nannan Guo and Ming C. Leu

Department of Mechanical and Aerospace Engineering  
Missouri University of Science and Technology, Rolla, MO 65409, USA

REVIEWED, Accepted August 16, 2012

## **Abstract**

Selective Laser Sintering (SLS) can be used to fabricate graphite composite bipolar plates with complex flow fields for Polymer Electrolyte Membrane (PEM) fuel cells. The additive manufacturing process can significantly reduce the time and cost associated with the research and development of bipolar plates as compared to other fabrication methods such as compression molding. In this study, bipolar plates with three different designs, i.e., parallel in series, interdigitated, and bio-inspired, were fabricated using the SLS process. The performance of these SLS-fabricated bipolar plates was studied experimentally within a fuel cell assembly under various operating conditions. The effect of temperature, relative humidity, and pressure on fuel cell performance was investigated. In the tests conducted for this study, the best fuel cell performance was achieved with a temperature of 75 °C, relative humidity of 100%, and back pressure of 2 atm.

## **1. Introduction**

A fuel cell is an electrochemical cell that converts chemical energy from a fuel and an oxidant into electrical energy. A typical fuel cell system can operate at 40-60% efficiency, while a fossil fuel power plant operates at only about 35% efficiency. Additionally, a fuel cell system can be made very compact and lightweight without moving parts. These unique advantages of a fuel cell provide it with many application opportunities. Several types of fuel cells exist, including the polymer electrolyte membrane (PEM) fuel cell, solid oxide fuel cell (SOFC), molten carbonate fuel cell (MCFC), direct methanol fuel cell, and so on. Compared to other types of fuel cells, the PEM fuel cell has great advantages including low-temperature operation, high-power density, fast start-up, system robustness, and low emissions.

A bipolar plate is a vital component in a PEM fuel cell. It supplies hydrogen and oxygen to reaction sites, removes the reaction product (i.e., liquid water) out of the fuel cell, collects the generated current, and provides mechanical support for the fuel cell. Bipolar plates constitute more than 60% of the weight and 30% of the total cost in a fuel cell stack [1]. The bipolar plate significantly influences the performance of a PEM fuel cell. For example, the electrical conductivity of the bipolar plate itself affects the fuel cell's internal resistance. The flow field design of the bipolar plate, which is used to transport reactants, greatly affects transport efficiency and, hence, fuel cell performance. Previous studies [2] have shown that the power density of a fuel cell can be increased significantly if the bipolar plate has a proper flow field design.

Bipolar plates usually are made of metal, graphite, and graphite composite. Metal has high electrical conductivity, but its poor chemical resistance does not allow it to persevere long within the chemical environment of a PEM fuel cell. Graphite has good electrical conductivity and chemical resistance, but its brittleness makes it very difficult to machine. Given the ease with which they can be manufactured and their excellent chemical resistance, graphite/polymer composites are becoming increasingly more promising for producing bipolar plates [3-10]. Two fabrication methods for massively producing these bipolar plates are injection molding (IM) [3] and compression molding (CM) [4]. Although these methods are suitable for mass production, they are not time-efficient or cost-effective for studying the bipolar-plate flow field design, which includes channel cross-section shapes, dimensions and layouts. In the IM and CM processes, the mold corresponding to each different design has to be fabricated, which is very expensive and time-consuming.

Selective Laser Sintering (SLS), as an additive manufacturing technology, has been studied to fabricate graphite composite bipolar plates for fuel cells [11-15]. Compared with CM and IM, SLS can fabricate graphite composite bipolar plates at a lower cost and shorter lead time, especially for the purpose of researching and developing new bipolar plate designs. In the SLS process, a mixture of graphite materials and binder in a powder bed is scanned by a laser, and the molten binder bonds graphite particles together to form 3D parts layer by layer. After a green part is built, it undergoes post-processing, including carbonization and infiltration, to increase the bipolar plate's electrical conductivity, mechanical strength and gas impermeability. Studies have been conducted to investigate the properties of the bipolar plates fabricated using different graphite materials [16]. However, the performance of fuel cells with SLS-fabricated bipolar plates has not been investigated, nor has the influence of different operating conditions on the performance of these fuel cells that use SLS-fabricated bipolar plates.

In this study, graphite composite bipolar plates with various flow fields, including parallel in series, interdigitated and bio-inspired designs, were fabricated using the SLS process. These fabricated bipolar plates were assembled in a PEM fuel cell unit. The performance of the fuel cells with these bipolar plates was studied experimentally under various operating conditions. The effects of temperature, relative humidity and pressure on fuel cell performance were investigated. The performance characteristics of fuel cells with different bipolar plate designs were compared. The long-term performance of the fuel cell using SLS-fabricated bipolar plates also was studied.

## **2. Experiments**

### **2.1 Materials**

Natural graphite (3610) and synthetic graphite (4437), obtained from Asbury Graphite Mills, Inc. (New Jersey, USA), were used to fabricate graphite composite bipolar plates. Natural graphite has high electrical conductivity but poor flowability due to its flaky shape. Synthetic graphite is a product made by treating amorphous carbon materials, usually calcined petroleum coke and coal tar pitch, at high temperatures. Because of its more uniform and spherical shape, synthetic graphite provides better flowability in a packed powder. The material composition in this study was 55vol% NG, 10vol% SG and 35vol% binder. Phenolic powder (GP-5546, Georgia

Pacific) with an average size of 15 $\mu$ m was used as the binder. The electrical conductivity was measured around 120 S/cm and the flexural strength around 40 MPa from a previous study [16]. After carbonization, porous brown parts were infiltrated with liquid epoxy resin (EPONTM Resin 828) in order to obtain gas impermeable parts.

## 2.2 Fabrication process

Graphite powder and phenolic binder were ball milled together for 12 hours to achieve a uniform mixture. An SLS machine (Sinterstation 2000) was used to build green parts from this mixture. The SLS process is depicted in Fig. 1. The CAD model of a bipolar plate was first converted into slices, and then the laser beam scanned the powder bed according to the cross-section of each slice (see Fig. 1). The binder, which has a low melting point, was melted by laser and bound the graphite particles. After one layer was scanned, the powder bed was lowered by one layer of thickness, and a new layer of the powder material was fed on the top. The process was repeated until the bipolar plate was fabricated completely. The parameters used in the SLS process were as follows: fill laser power (14 W), outline laser power (4 W), laser scan speed (1.5 m/s), layer thickness (0.1 mm), and laser scan spacing (0.08 mm). The temperatures of the part bed and feed bins were maintained at 60 °C and 40 °C, respectively. For carbonization, green parts were heated to 1000 °C in a furnace filled with Argon gas to dissociate the binder and convert it to carbon residue to get brown parts. The heating schedule was from room temperature to 200 °C with a heating ramp rate of 60 °C/h, followed by a slower rate of 30 °C/h to 600 °C, and then a 50 °C/h ramp rate to 1000 °C, maintained for 1 h. Brown parts, which are porous and weak, must be infiltrated with a liquid resin to become gas impermeable and to increase their mechanical strength. For infiltration, porous brown parts were immersed into the mixture of liquid epoxy resin and a curing agent, taken out after 20 min for their surfaces to be cleaned, and then placed in an oven at 80 °C for 30 min to cure the infiltrated resin.

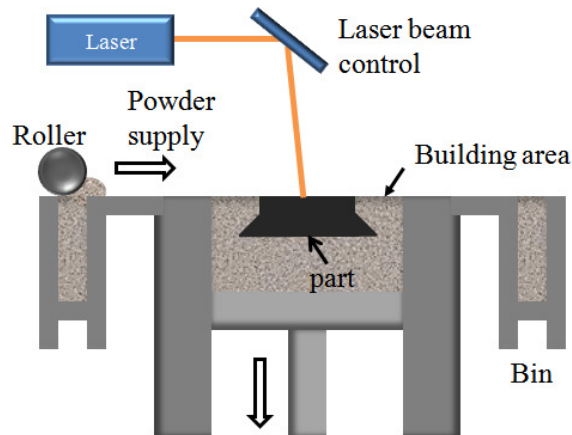


Figure 1. Fabrication process of Selective Laser Sintering.

## 2.3 Bipolar plate designs

Three flow patterns (parallel in series, interdigitated and bio-inspired designs) were developed in this study. The parallel in series design (Figure 2(a)) consisted of four sets of connected parallel channels with a channel width of 1.5 mm and a land width (distance between two adjacent channels) of 1.0 mm. The interdigitated design (Figure 2(b)) was composed of two

sets of parallel channels, one of which was connected to the inlet, and the other to the outlet. These two sets of channels were interdigitated together but not directly connected. In this design, reactants are forced to flow through the gas diffusion layer (GDL) under the land area, which increases the reactant concentration on the catalyst surface; however, an excessive pressure drop is required. The channel width was 1.5 mm and the land width was 1.0 mm in this design. The bio-inspired design (Figure 2(c)) was inspired by the vein structures of leaves, which transport mass efficiently from one central source to the whole surface of a leaf, mirroring the function of bipolar plate flow fields. The leaf vein structure was mimicked in bio-inspired design with three generations of channels: the primary, secondary and tertiary generations. The width of all of these channels was 1.5 mm in order to achieve a fair comparison with the other two designs. At the end of all of the channels, the remaining reactant is forced to flow through the land area and merge to the outlet. The active area, thickness of bipolar plates, and channel depth of all three designs were the same at 50×50 mm<sup>2</sup>, 3.0 mm and 1.5 mm, respectively. All the three bipolar plate designs were fabricated using the SLS process. The fabricated bipolar plates are shown in Figure 3.

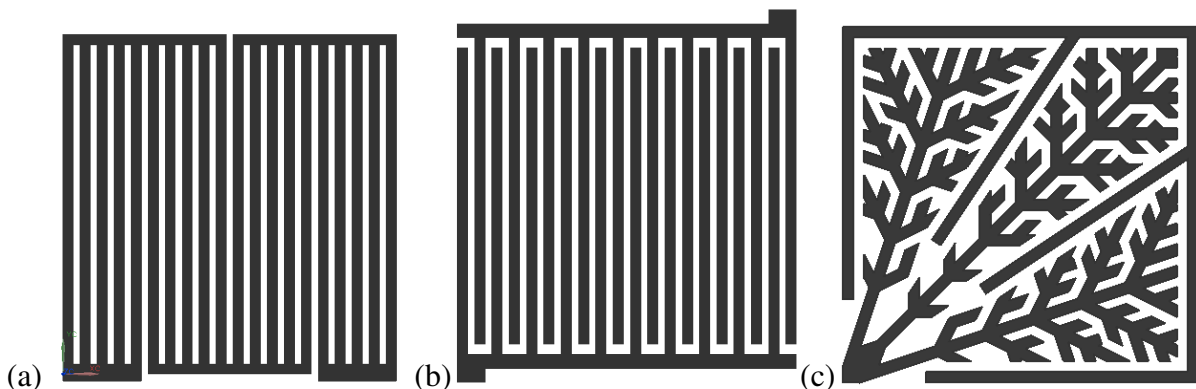


Figure 2. Bipolar plates with different flow field designs: (a) parallel in series design; (b) interdigitated design; (c) bio-inspired design.

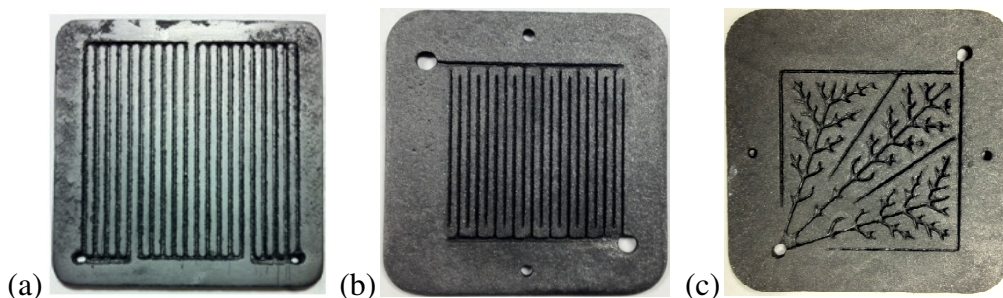


Figure 3. Bipolar plates with different flow field designs fabricated using the SLS process: (a) parallel in series design; (b) interdigitated design; (c) bio-inspired design. All three bipolar plates have an active area of 50×50 mm<sup>2</sup>.

## 2.4 Fuel cell testing

A single fuel cell unit was assembled using two fabricated bipolar plates, two end plates, and one commercial membrane electrode assembly (MEA), as shown in Figure 4. Two gold-plated copper plates were used to collect the generated current. The MEA (from FuelCellsEtc) comprises a loading of 4 mg/cm<sup>2</sup> platinum as the catalyst on both the anode and cathode sides,

Nafion<sup>®</sup> 115 as the membrane, and carbon cloth as the gas diffusion layer (GDL). Fuel cell performance was measured using a test station (Greenlight Innovation, G40) under different operating conditions in order to study the effects of temperature, humidity, and pressure. The temperature varied from 55 °C to 85 °C, the relative humidity for both the anode and cathode varied from 0 to 100%, and the back pressure varied from 0 to 2 atm. Table 1 provides details about the experimental designs. A thermocouple mounted inside the end plate was used to measure the temperature of the fuel cell. The flow rates of the anode and cathode were controlled by two separate mass flow controllers and were 0.3 Lpm and 1.05 Lpm, respectively, for all of the experiments. The relative humidity was controlled by adjusting the dew point temperature of the inlet flow. After the operating temperature and humidity were set, it took 90-120 minutes on average to reach the steady state. After that, testing began by increasing the current density at each step and recording the corresponding voltage after two minutes (making sure the output was steady). The increase in current density continued until the cell voltage dropped to 0.3 V. After that, the current density was set back to zero, and two more tests were performed. The final data for each condition was obtained by taking the average of the three tests. The power density was obtained by multiplying the current density and the corresponding voltage.

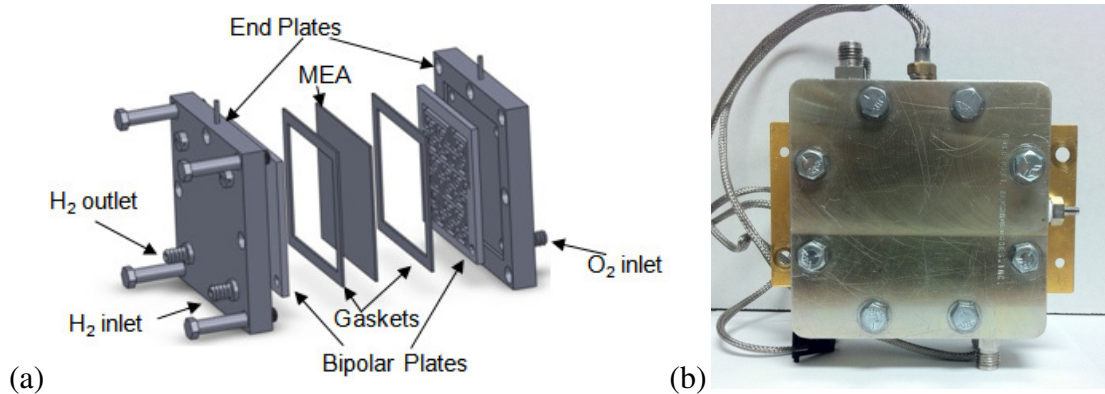


Figure 4. (a) Major components in a PEM fuel cell; (b) Actual fuel cell assembly used in the experiments.

Table 1. Operating conditions for fuel cell testing experiments.

	Temperature (°C)	Relative humidity		Back pressure (atm)
		Anode	Cathode	
Group A (temperature)	55	100%	100%	0
	65	100%	100%	0
	75	100%	100%	0
	85	100%	100%	0
Group B (relative humidity)	75	25%	25%	0
	75	50%	50%	0
	75	75%	75%	0
	75	100%	100%	0
Group C (back pressure)	75	100%	100%	0
	75	100%	100%	1
	75	100%	100%	2

### 3. Results and Discussion

#### 3.1 Effect of temperature

The performance of a PEM fuel cell is characterized by its polarization curve, which is the curve of voltage versus current density. Figure 5 shows the polarization curve as well as the curve of power density versus current density under different temperatures for the three flow field designs. The performance of the fuel cell shows a typical polarization curve, indicating that the graphite composite bipolar plates fabricated using the SLS process are satisfactory for application to PEM fuel cells. All of the results show that, initially, the power density continually increases as the current density increases, reaching the maximum value when the current density is around 900 mA/cm<sup>2</sup>. As shown in Figure 5, the performance of the fuel cell greatly increases when the temperature increases from 55 °C to 65 °C. After reaching 65 °C, the performance of the fuel cell remains almost the same from 65 °C to 75 °C, and then decreases from 75 °C to 85 °C. All three designs show this similar trend in terms of the influence of temperature. The parallel in series design experiences a large increase from 55 °C to 65 °C and a significant drop from 75 °C to 85 °C, but for the interdigitated and bio-inspired designs, the differences between the two ranges of temperatures are relatively small. According to the fuel cell theory, the actual voltage output of a fuel cell equals the thermodynamic voltage subtracted by the various overvoltage losses [17]:

$$V = E_T - \eta_{act} - \eta_{ohmic} - \eta_{conc} \quad (1)$$

where  $V$  is the real voltage output of a fuel cell,  $E_T$  is the thermodynamic voltage of a fuel cell at temperature  $T$ ,  $\eta_{act}$  represents activation losses due to reaction kinetics,  $\eta_{ohmic}$  represents ohmic losses from ionic and electronic resistance, and  $\eta_{conc}$  represents concentration losses due to poor mass transport. The effect of temperature on the voltage output has two parts, one on thermodynamic voltage  $E_T$  and the other on activation losses  $\eta_{act}$ . The relationship between the thermodynamic voltage and temperature is given by:

$$E_T = E^0 + \frac{\Delta\hat{s}}{nF}(T - T_0) \quad (2)$$

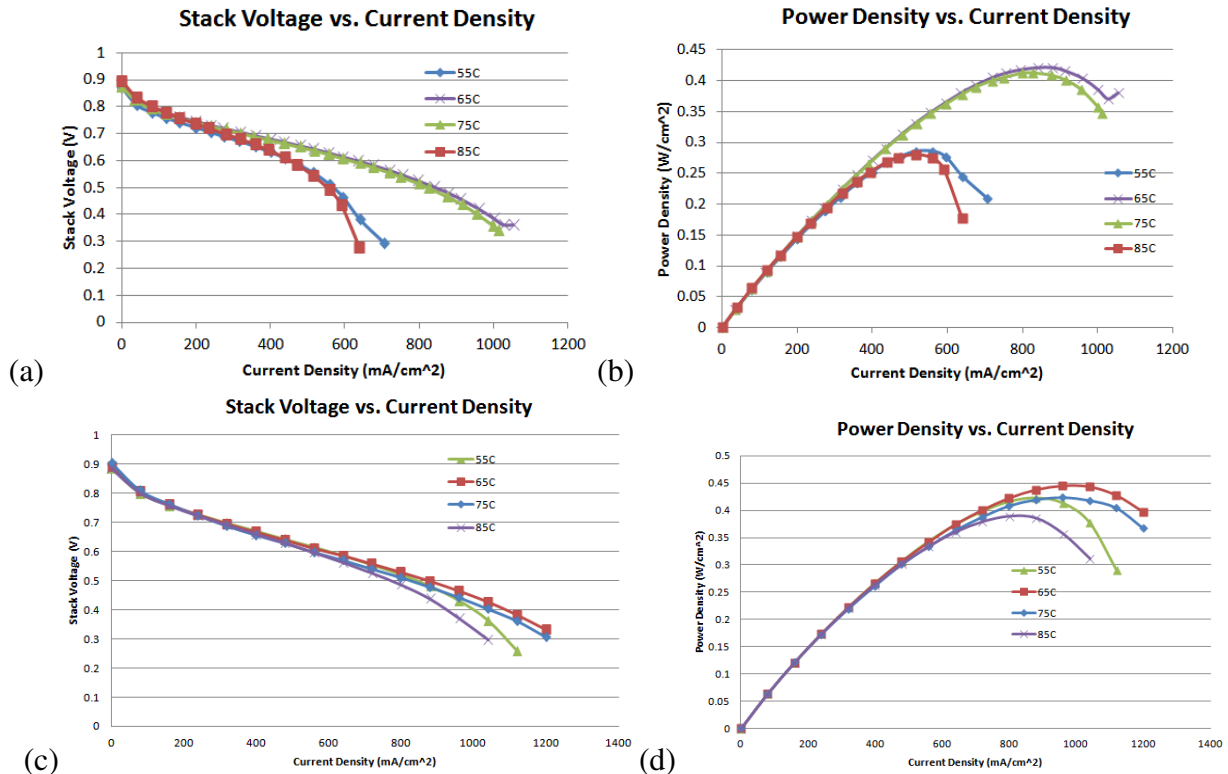
where  $E^0$  is the thermodynamic voltage under standard-state conditions (25 °C and 101.325 KPa),  $\Delta\hat{s}$  is the change in entropy for the chemical reaction, which is negative for most fuel cell reactions,  $n$  is the number of moles of electrons transferred, and  $F$  is Faraday's constant. As Equation (2) reveals, because  $\Delta\hat{s}$  is negative for the PEM fuel cell reaction, the thermodynamic voltage will decrease as the temperature increases. An increase in temperature also will reduce activation losses (due to reaction kinetics) due to the increase in exchange current density as the temperature increases. This is because increasing the reaction temperature will increase the thermal energy available in the system, and all of the particles in the molecule will move and vibrate with increased intensity. This higher level of thermal activity increases the likelihood that a given reactant will possess sufficient energy to reach the activated state, thus increasing the rate of reaction and decreasing activation losses. This dynamic can be expressed in the Butler-Volmer equation (Equation (3)) and the definition of exchange current density (Equation (4)), i.e. [18]:

$$j = j_0 \left( \frac{c_R^*}{c_R^{0*}} e^{\frac{\alpha n F \eta_{act}}{RT}} - \frac{c_P^*}{c_P^{0*}} e^{\frac{-(1-\alpha) n F \eta_{act}}{RT}} \right) \quad (3)$$

where  $c_R^*$  is the reactant concentration,  $c_P^*$  is the product concentration,  $c_R^{0*}$  and  $c_P^{0*}$  are the reference concentrations of the reactant and product,  $\alpha$  is the transfer coefficient, and  $j_0$  is the reference exchange current density, which is given by:

$$j_0 = nF c_R^* f_1 e^{-\Delta G_1^\ddagger / (RT)} \quad (4)$$

where  $f_1$  is the decay rate from reactants to products, and  $\Delta G_1^\ddagger$  is the activation barrier for the forward reaction. The Butler-Volmer equation states that the current produced by an electrochemical reaction increases exponentially with activation overvoltage, which is sacrificed to overcome the activation barrier associated with the electrochemical reaction. Therefore, if more current is drawn from the fuel cell, more activation overvoltage is lost. If the exchange current density  $j_0$  is increased to draw the same amount of current density from the fuel cell, less activation overvoltage will be needed. As Equation (4) indicates, increasing the temperature exchange will increase the current density exponentially, thus reducing activation losses. Therefore, the effect of temperature on fuel cell performance is the compromise of these two opposite influences, i.e., negative on thermodynamic voltage and positive on activation losses. When the temperature increases, the positive influence on the reduction of activation losses initially is greater than the negative influence on the reduction of thermodynamic voltage. Therefore, the overall performance of the fuel cell increases. However, after the temperature exceeds 65 °C, these two effects begin to merge, and the overall fuel cell performance barely changes from 65 °C to 75 °C. Finally, the negative effect will surpass the positive effect, inhibiting the performance of the fuel cell as the operating temperature increases. The experimental results for these different flow field designs agree well with the theoretical analysis and show that the range of 65 °C to 75 °C is the optimal operating temperature for all of these designs.



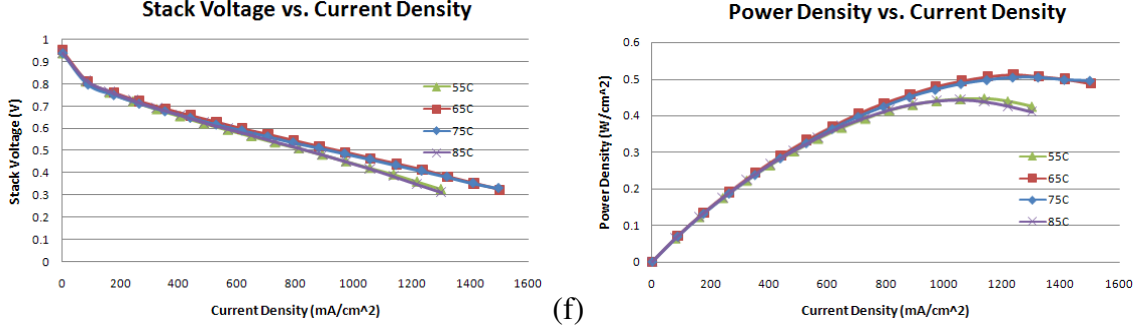


Figure 5. Effect of temperature on fuel cell performance (Group A). The relative humidity was kept at 100%, and back pressure at 0 atm: (a, b) parallel in series design, (c, d) interdigitated design and (e, f) bio-inspired design.

### 3.2 Effect of relative humidity

The performance of fuel cells with graphite composite bipolar plates fabricated using the SLS process was investigated under different relative humidity, with the temperature kept at 75 °C and the back pressure at 0 atm. The experimental results for fuel cells with different designs are shown in Figure 6. Figure 6(a, c, e) shows the polarization curves under different relative humidity, and Figure 6(b, d, f) shows the corresponding power density curves. As indicated, relative humidity has a significant effect on fuel cell performance. The power density increased greatly as humidity increased from 25% to 75%; the rate of this increase slowed slightly after reaching 75%. The power density increased approximately 4-8 times when the humidity increased from 25% to 100%. All of the performance charts of fuel cells using the three different flow field designs show this same trend.

Relative humidity mainly affects the ionic resistance of the polymer electrolyte (Nafion) because Nafion has to be hydrated by liquid water in order to maintain high proton conductivity. The relationship between the proton conductivity of Nafion and water content is as follows [19]:

$$\sigma = (0.005193\lambda - 0.00326)\exp \left[ 1268 \left( \frac{1}{303} - \frac{1}{T} \right) \right] \quad (5)$$

where  $\sigma$  is the conductivity of Nafion,  $\lambda$  is the water content, and  $T$  is the temperature. According to Equation (5), the proton conductivity of Nafion increases linearly with increase in its water content  $\lambda$ , which occurs when the operating humidity increases. As a result, the fuel cell performance increases greatly with an increase in humidity, as seen in Figure 6, because of the reduction of ohmic losses. The water content in Nafion is defined as the ratio of the number of water molecules to the number of charged sites ( $SO_3^-H^+$ ), which can be estimated from the humidity condition of a fuel cell using the following formula [19]:

$$\lambda = \begin{cases} 0.0043 + 17.81a_w - 39.85a_w^2 + 36.0a_w^3, & 0 < a_w \leq 1 \\ 14 + 1.4(a_w - 1), & 1 < a_w \leq 3 \end{cases} \quad (6)$$

where  $a_w$  is the relative humidity defined by:

$$a_w = \frac{p_w}{p_{SAT}} \quad (7)$$

where  $p_w$  is the actual partial pressure of water vapor in the fuel cell's system, and  $p_{SAT}$  represents the saturation water vapor pressure at the fuel cell's operating temperature. The

experimental results from the PEM fuel cells using SLS-fabricated bipolar plates agree well with the theoretical analysis of the effect of relative humidity on fuel cell performance.

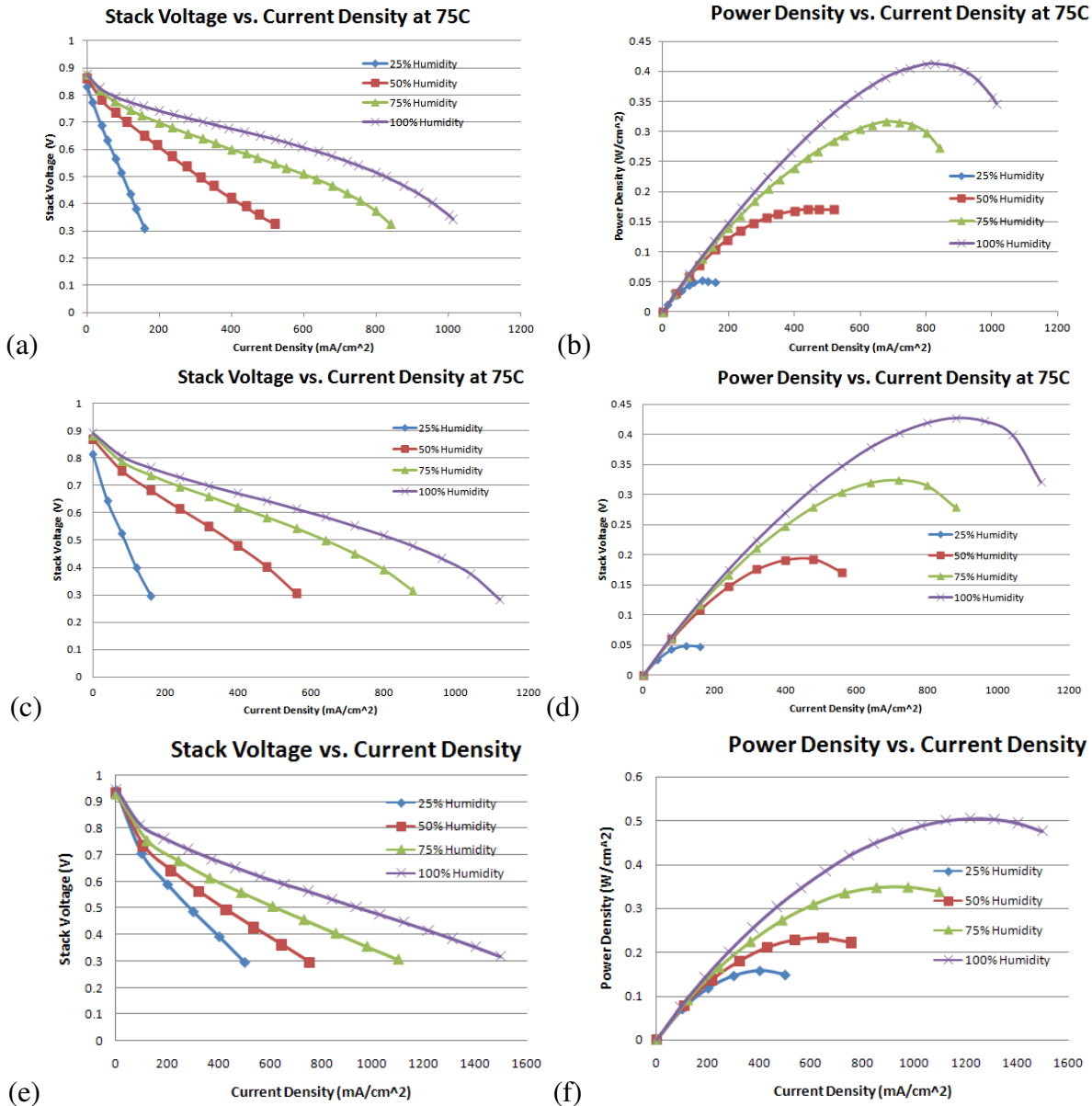


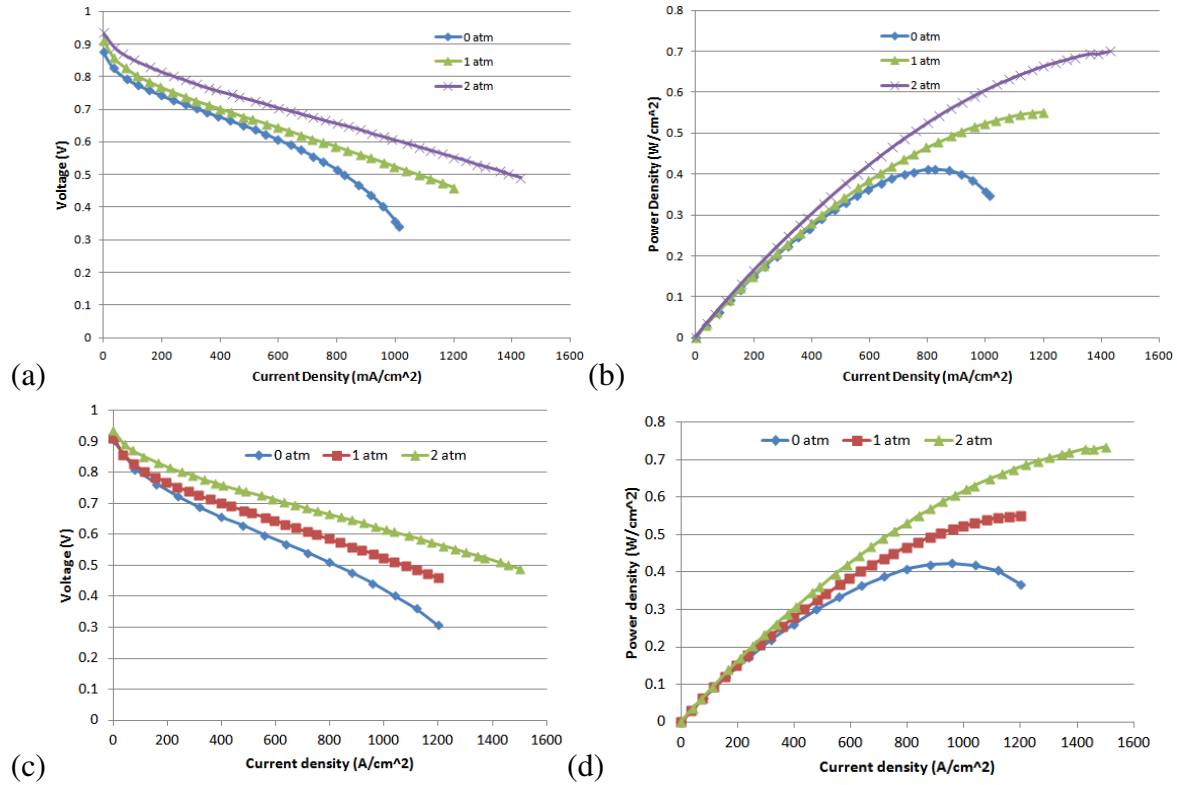
Figure 6. Effect of relative humidity on fuel cell performance (Group B). Temperature was maintained at 75 °C and back pressure at 0 atm: (a, b) parallel in series design, (c, d) interdigitated design and (e, f) bio-inspired design.

### 3.3 Effect of back pressure

Figure 7 shows the effect of back pressure on the performance of fuel cells using the parallel in series design (a, b), interdigitated design (c, d), and bio-inspired design (e, f). The results show that the performance of the PEM fuel cell increases greatly as the back pressure increases from 0 atm to 2 atm. This occurs because the increase of back pressure will increase the reactant concentration at both the anode and cathode, according to the following equation:

$$C_R^* = \frac{N}{V} = \frac{P}{RT} \quad (8)$$

The reactant concentration will greatly increase the reaction rate (Equation 4), thus increasing fuel cell performance. Additionally, the high back pressure applied on the outlet of the flow field will force the reactants to flow into the porous gas diffusion layer (GDL), which also improves the mass transport towards the catalyst layer. Therefore, more reactants will take part in the electrochemical reaction, resulting in higher performance. The high back pressure also benefits the removal of water droplets formed within the GDL and keeps the fuel cell from flooding [20]. Figure 7(a) shows that the mass transport loss becomes prominent when the current density rises above 600 mA/cm<sup>2</sup> for zero back pressure in the parallel in series design, while at pressures of 1 atm and 2 atm, the mass transport loss shows no remarkable increase even when the current density is as high as 1200 mA/cm<sup>2</sup>. The power density curve also demonstrates this point. The power density began to decrease when the current density rose above 800 mA/cm<sup>2</sup> at a back pressure of 0 atm, but it continuously increased at back pressures of 1 atm and 2 atm. Similar trends were observed on the effect of back pressure for the other two bipolar plate designs.



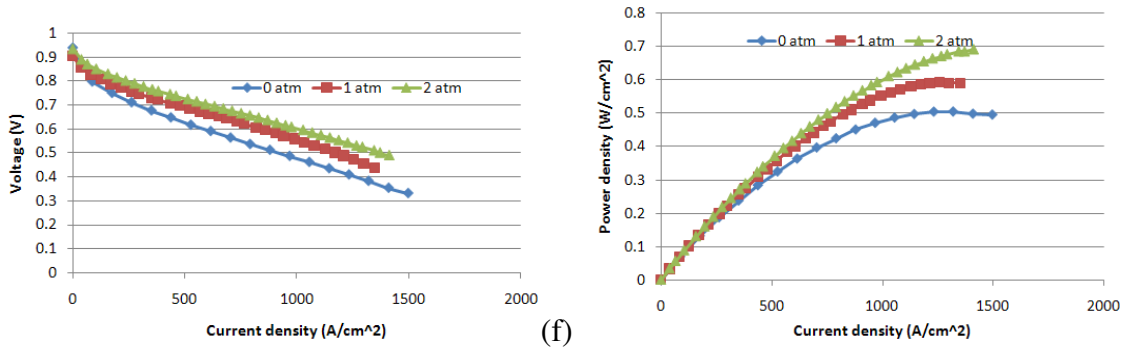


Figure 7. Effect of back pressure on fuel cell performance (Group C). Temperature was maintained at 75 °C and relative humidity at 100%: (a, b) parallel in series design, (c, d) interdigitated design and (e, f) bio-inspired design.

### 3.4 Comparison of performance for different flow field designs

Figure 8 shows the performance comparison of PEM fuel cells using different bipolar plate flow field designs. Polarization curves and power density curves are shown in Figure 8(a) and (b), respectively. The bio-inspired design performed best among the three flow field designs, with a maximum power density of around 0.5 W/cm<sup>2</sup>. This is due to the higher mass transport capability of the bio-inspired design, which can be seen from the polarization curves that indicate less mass transport loss associated with this design. The maximum power density of the interdigitated design was 0.43 W/cm<sup>2</sup>, which was slightly higher than that of the parallel in series design. The polarization curves show that the parallel in series design initially performed very similarly to the interdigitated and bio-inspired designs; at the middle region, it even exhibited slightly higher performance than the other designs. These findings indicate that the parallel in series design had a relatively high contact electrical conductivity between the bipolar plates and GDLs. However, after the current density increased above 800 mA/cm<sup>2</sup>, the parallel in series design suffered from a larger mass transport loss due to insufficient mass supply, while the performance of the interdigitated and bio-inspired designs did not drop sharply because of their better mass transport ability. Eventually, the bio-inspired design performed better than the other two designs, indicating that it has the most efficient transport ability.

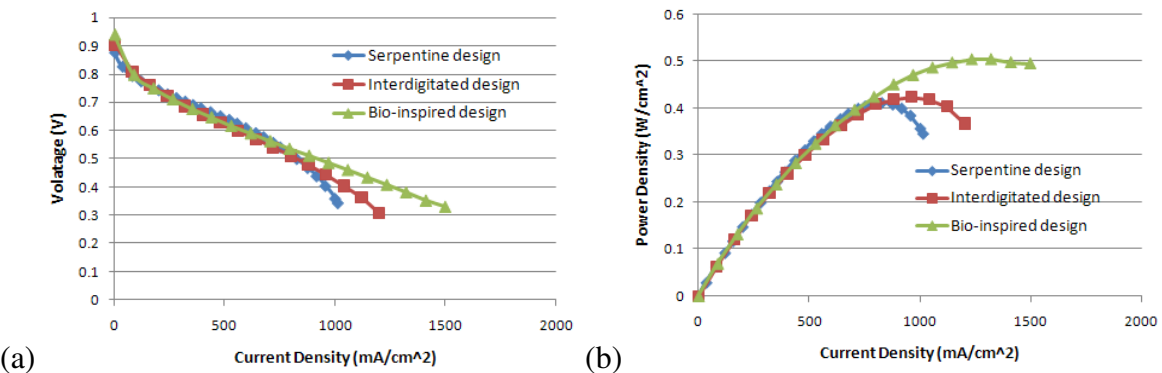


Figure 8. Comparison of the performance of fuel cells with different flow field designs (parallel in series, interdigitated and bio-inspired) under the same operating conditions (temperature of 75 °C, relative humidity of 100% and back pressure of 0 atm).

### 3.5 Fuel cell long-term performance test

The long-term performance of PEM fuel cells using SLS fabricated bipolar plates was also investigated to study the long-term work capability of the fabricated graphite composite bipolar plates. The parallel in series design was used in this study, with the operating conditions set to 75 °C, 100% relative humidity, and zero back pressure. After steady operating conditions had been reached, the performance of the fuel cell was recorded every 10 seconds for 6 hours. The result is shown in Figure 9, in which the x axis is the operating time and the y axis is the variation of the cell voltage, while a constant current density of 750 mA/cm<sup>2</sup> is drawn out from the fuel cell by the test station. This current density is the point at which the fuel cell with the parallel in series design can produce the maximum power density, as shown in Figure 8(b). From the result shown in Figure 9(a), the voltage continuously increased over the first 120 minutes from 0.515 V to 0.535 V; after that, the cell voltage remained relatively steady at 0.535 V, with very little variation, around  $\pm 0.005$  V. The fuel cell achieved its steady state around 120 minutes after the pre-set operating conditions had been reached. This is why, in all of the experiments, the tests were started 120 minutes after the operating conditions were reached, as described in Section 2.3. Figure 9(b) details the performance from the 170<sup>th</sup> minute to the 179<sup>th</sup> minute. The voltage decreased suddenly around the 174<sup>th</sup> minute; 80 ms later, it returned to the steady-state voltage; then, around the 176<sup>th</sup> minute, another small drop occurred. These voltage drops were caused by the accumulation of liquid water in the flow channels. When the liquid water was removed from the fuel cell by the flow of the reactants, which can be observed from the transparent outlet pipe, the voltage returned to the steady state. Then, once again, the liquid water slowly accumulated inside the flow field, thus decreasing the voltage, and suddenly the voltage increased to the normal value as the water was dragged out of the channels. This result indicates that the SLS-fabricated bipolar plates could provide a fuel cell with a steady, long-term performance.

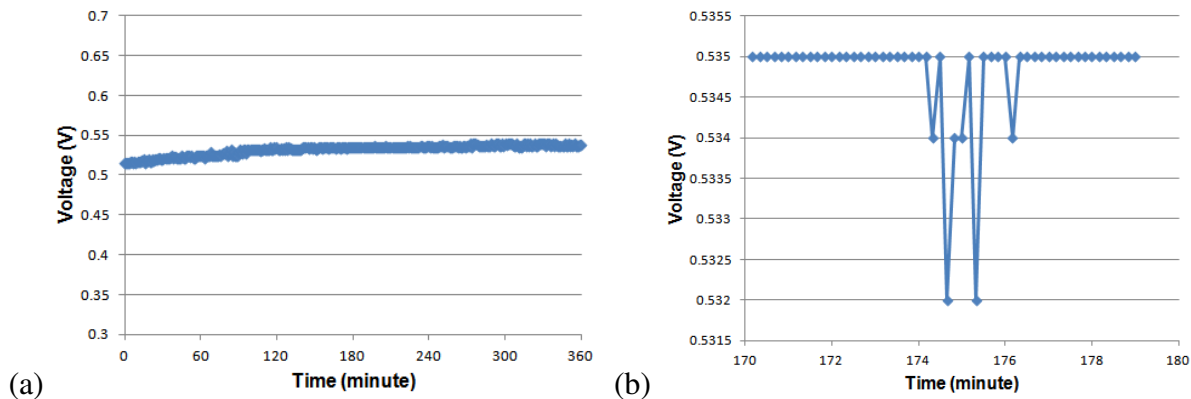


Figure 9. (a) Six-hour performance of the PEM fuel cell with SLS-fabricated graphite composite bipolar plates; (b) a detailed performance plot from the 170th minute to the 179th minute.

## 4. Conclusions

Graphite composite bipolar plates were fabricated using the Selective Laser Sintering process, which can make flow fields with complicated geometries. The fabricated bipolar plates were assembled into a fuel cell unit whose performance was tested under different operating conditions, with the temperature varying from 55 °C to 85 °C, relative humidity from 25% to

100%, and back pressure from 0 atm to 2 atm. The effects of temperature, relative humidity, and back pressure on the performance of PEM fuel cells were investigated. Fuel cell performance increased initially when the temperature increased from 55 °C to 75 °C, but after that, the performance decreased with increases in temperature. Both relative humidity and back pressure had a significant effect on the performance of fuel cells; the higher the humidity or back pressure, the higher the power density of the fuel cell. An analytical model based on PEM fuel cell thermodynamics and electrochemistry was used to help explain these experimental results. The performance characteristics of fuel cells using the parallel in series, interdigitated, and bio-inspired bipolar designs also were compared against each other, and the results show that the bio-inspired design performed best. The long-term operation of the PEM fuel cell with the SLS fabricated bipolar plates produced a very stable output, indicating that there was no water flooding within the flow field.

### **Acknowledgement**

This project is funded by the National Science Foundation grant #CMMI-1131659.

### **References**

- [1] Tsuchiya, H., Kobayashi, O. Mass production cost of PEM fuel cell by learning curve. *Int. J. Hydrogen Energy*, 2004, 29: 985-990.
- [2] Kloess, J. P., Wang, X., Liu, J., Shi, Z., Guessous, L. Investigation of bio-inspired flow channel designs for bipolar plates in proton exchange membrane fuel cells. *Journal of Power Sources*, 2009, 188: 132-140.
- [3] Muller, A., Kauranen, P., Ganski, A., Hell, B. Injection moulding of graphite composite bipolar plates. *Journal of Power Sources*, 2006(154): 467-471.
- [4] Dhakate, S. R., Mathur, R. B., Kakati, B. K., Dhami, T. L. Properties of graphite-composite bipolar plate prepared by compression molding technique for PEM fuel cell. *International Journal of Hydrogen Energy*, 2007, 32: 4537-4543.
- [5] Mathur, R. B., Dhakate, S. R., Gupta, D. K., Dhami, T. L., Aggarwal, R. K. Effect of different carbon fillers on the properties of graphite composite bipolar plate. *Journal of Materials Processing Technology*, 2008, 203: 184-192.
- [6] Blunk, R., Elhamid, M. H., Lisi, D., Mikhail, Y. Polymeric composite bipolar plates for vehicle application. *Journal of Power Sources*, 2006, 156: 151-157.
- [7] Du, L., Jana, S. C. Highly conductive epoxy/graphite composites for bipolar plates in proton exchange membrane fuel cells. *Journal of Power Sources*, 2007, 172: 734-741.
- [8] Lee, J. H., Jang, Y. K., Hong, C. E., Kim, N. H., Li, P., Lee, H. K. Effect of carbon fillers on properties of polymer composite bipolar plates of fuel cells. *Journal of Power Sources*, 2009, 193: 523-529.
- [9] Hsiao, M. C., Liao, S. H., Yen, M. Y., Su, A., Wu, I. T., Hsiao, M. H., Lee, S. J. Effect of graphite sizes and carbon nanotubes content on flowability of bulk-molding compound and formability of the composite bipolar plate for fuel cell. *Journal of Power Sources*, 2010, 195: 5645-5650.
- [10] Yen, C. Y., Liao, S. H., Lin, Y. F., Huang, C. H., Lin, Y. Y., Ma, C. M. Preparation and properties of high performance nanocomposite bipolar plate for fuel cell. *Journal of Power Sources*, 2006, 162: 309-315.

- [11] Guo, N., Leu, M. C. Effect of different graphite materials on electrical conductivity and flexural strength of bipolar plates fabricated by selective laser sintering. International SFF Symposium, Austin, 2010.
- [12] Chen, S., Bourell, D. L., Wood, K. L. Fabrication of PEM fuel cell bipolar plates by indirect SLS. International SFF Symposium, Austin, 2004.
- [13] Chen, S., Murphy, J., Herlehy, J., Bourell, D. L. Development of SLS fuel cell current collectors. Rapid Prototyping Journal, 2006: 275-282.
- [14] Wu, M., Leu, M. C., Guo, N. Simulation and Testing of Polymer Electrolyte Membrane Fuel Cell Bipolar Plates Fabricated by Selective Laser Sintering. Proceedings of ASME 2012 International Symposium on Flexible Automation, St. Louis, 2012.
- [15] Bourell, D. L., Leu, M. C., Chakravarthy, K., Guo, N., Alayavalli, K. Graphite-based indirect laser sintered fuel cell bipolar plates containing carbon fiber additions. CIRP Annals – Manufacturing Technology, 2011, 60: 275-278.
- [16] Guo, N., Leu, M.C. Effect of different graphite materials on the electrical conductivity and flexural strength of bipolar plates fabricated using selective laser sintering. International Journal of Hydrogen Energy, 2012, 37: 3558-3566.
- [17] O'hayre, R. P., Cha, S. W., Colella, W. G., Prinz, F. B. Fuel cell fundamentals. 2nd ed. John Wiley & Sons, Inc., Hoboken, New Jersey, 2009, pp195-197.
- [18] Bard, A. J., Faulkner, L. R. Electrochemical Methods (2<sup>nd</sup> ed.). John Wiley and Sons, New York, 2001.
- [19] Springer, T. E., Zawodzinski, T. A., Gottesfeld, S. Polymer electrolyte fuel cell model. Journal of the Electrochemical Society, 1991, 138(8): 2334-2342.
- [20] Li, H., Tang, Y., Wang, Z., Shi, Z., et al. A review of water flooding issues in the proton exchange membrane fuel cell. Journal of Power Sources, 2008, 178: 103-117.